Norwegian University of Science and Technology

TMM4511 MATERIALS SPECIALIZATION PROJECT

ADHESION OF METAL-COMPOSITE JOINTS

EUROPEAN COPATCH PROJECT

Author:
Audun Reinsborg Log

Supervisor:
Andreas Echtermeyer

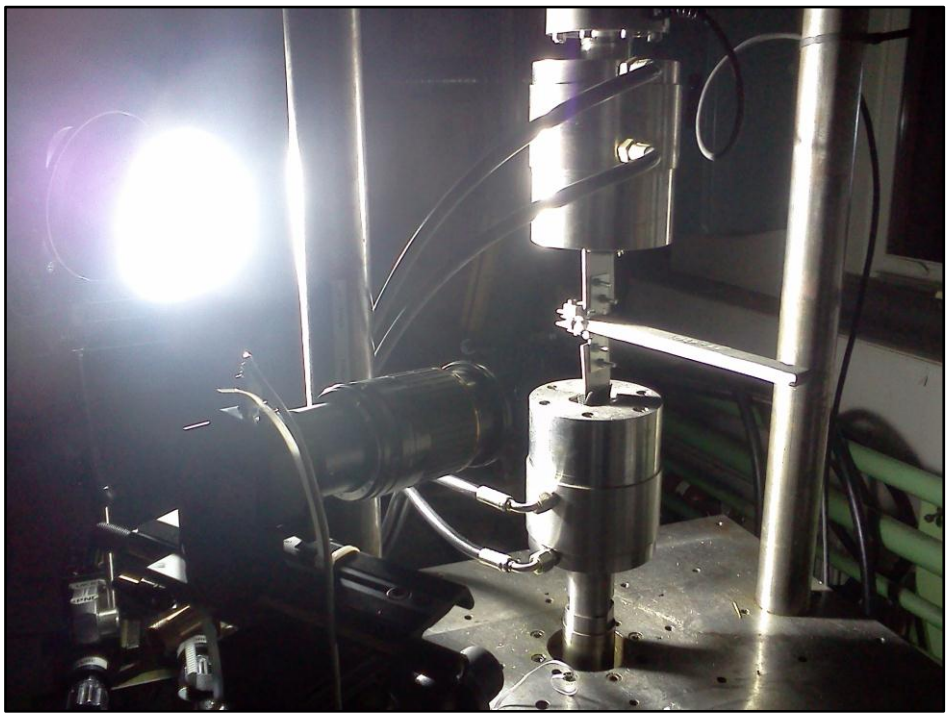

Preface

This report is written as a part of the TMM4511 Materials, Specialization Project at the Department of Engineering Design and Materials. Initial ambition of working with product development has given a background and grown an interest in mechanical analysis and materials science. When choosing a project, the Co-Patch project stood out as an extensive initiative for a technology with clear advantages. In addition, the opportunity for practical application of theory combined with analysis was also important, and I wish to continue the work of this project for my master thesis. The complimentary courses chosen were TMM6 Composite Structures and TMM9 Design for Structural Integrity. These were the most relevant for the project.

I would like to thank PhD.-candidate John Harald Grave for extensive help in material acquisition, production and analysis of test specimens and to PhD.-candidates Giovanni Perillo and Jan Peder Hegdal for instructions on equipment in the fatigue lab.

At last I would like to thank supervisor Andreas Echtermeyer for advice on procedure and interpretation of results.

Abstract

The Co-Patch project is searching to define a standard for composite patching for reinforcing or repairing damaged steel members of marine or civil infrastructure. This project tests different surface treatments and methods of interface application to quantitatively compare and find the procedure with best mechanical properties. The interface is a glass fibre layer. The two surface treatments are tested are grit blasting and needle gun. The two application methods tested were epoxy applied onto glass fibre cloth in wet layup then cured before carbon fibre application and pre-impregnated glass fibre applied directly before carbon fibre application. Conditions were tested using Double Cantilever Beam and End-Notched Flexure.

Batches treated with needle scaler delaminated directly after cutting. Specimen which did not delaminate showed poor adhesion. Batches with glass fibre applied with wet layup showed the highest results in mode I testing with a mean value of 1 333 J/m^2. The mode II testing showed a smaller difference, pre-impregnated glass fibre showing a slightly higher value of 982 J/m^2**.**

Different compliance calibrations were tested. One 3-point compliance calibration for each specimen tested at one crack length and one 8-point batch compliance calibration conducted for the two first specimen of each batch. Both showed significant deviations due to tests of the same crack length measuring different compliance.

A modelling approach is proposed which render few convergence problems, has the ability to fit test data, and requires only a few parameters. Higher dependency on these parameters makes it less flexible.

A fatigue approach has been investigated for similar tests and specimens have been made and are ready for testing.

Table of contents

List of figures

List of tables

Nomenclature

ENF	End notched flexure
DCB	Double cantilever beam
K_{tt}	Penalty stiffness, transverse
K_{nn}	Penalty stiffness, normal
S_{tt}	Interface strength, transverse
S_{nn}	Interface strength, normal
δ_f	Separation failure
N_e	Number of elements in cohesive zone
l_e	Cohesive element length
l_{cz}	Cohesive zone length
δ	Displacement
G_I	Strain energy release rate, mode I
G_{II}	Strain energy release rate, mode II
G_{III}	Strain energy release rate, mode III
G_C	Critical strain energy release rate
VCCT	Virtual crack closure
CZM	Cohesive zone modeling
σ	Standard deviation
μ	Average
υ	Poisson's ratio
C	Compliance
P	Force applied
t_s	Thickness steel
t_{cf}	Thickness carbon fiber
w	Specimen width
υ_f	Fiber volume fraction
E	Young's modulus

1 Introduction

The Co-Patch project is a European funded project on Composite Patch Repair for Marine and Civil Engineering Infrastructure Applications. It is collaboration between 15 organizations from eight European countries to develop a standard on patching cracks in metal constructions and reinforce components by the use of composite materials.

Benefits of using composite patch repairs:

- Low weight on added material
- High fatigue resistance compared to welded/bolted joints
- No added stress concentrations
- No hot work required allowing application in explosive environment
- Direct application after a simple surface preparation
- Can be completed fast

The method of patching fractured steel members and it's structural properties as a reinforcement is significantly dependent on the adhesive bonding. To quantitatively compare different surface treatments, materials and application methods, and to establish design constants for damage analysis, testing in actual modes present will be conducted. These are mainly mode I and mode II. For testing of pure mode I fracture the recommended procedure is using double cantilever beam specimen and end notched flexure specimen for pure mode II fracture. A model based on the results from testing shall be constructed using finite element analysis. In addition, a fatigue assessment procedure shall be established and tried.

2 Theory

Tests will be on fracture of the adhesive layer between the steel and composite. Data acquisition and reduction depends on the fracture mode. Different procedures are required as explained in the following.

2.1 Adhesion

Adhesives are substances used to join two components together. The components are often referred to as substrates or adherends. The adhesive should have the thermodynamic properties to form intimate contact with both adherends and to coalesce. The physics used to explain the bond strength have been tied with dispersion of van der Waal forces, chemical bonds, molecular inter-diffusion for similar materials, electrical double layers leading to electrostatic attraction and mechanical adhering through interlocking the adhesive within crevices of adherend surface. To enhance the mechanical adhering, surface treatments are used to remove weakly bound surface layers and to create more and larger pores for interlocking. [1]

Breaking the attraction force between atoms of adhesive and adherend release energy is known as thermodynamic work of adhesion, measured in [J/m2]. When testing larger systems, however, energy is also dissipated into bulk and extrinsic deformations, yielding much higher values than just theoretical work of adhesion.

2.2 Fracture mechanics

Fracture mechanics is the characterisation of a material's resistance to fracture by the use of analytical solid mechanics and testing. As described by Dillard and Pocious [2], a fracture occurs if cohesive tractions in an adhesive interface are sufficiently large so as to induce non-linear irreversible deformation. The tractions are provided by potential energy between atoms of adherend and adhesive as the atoms are separated. The reduction in this potential energy between two surfaces is equal to the total strain energy, *dU*. As a material parameter for engineering purposes, the density of strain energy released is desired. A measure of this is the energy release rate, *G*, which relates the strain energy change to the crack propagation, the *cohesive zone*, as described by Griffith [3].

$$G = \frac{dU}{da} \tag{2.1}$$

This is related to the frequently used material parameter fracture toughness of plane stress or plane strain, K, by the equation

$$G_I = \frac{K_I}{E'} \tag{2.2}$$

Cracks are known to develop in three different, independent modes.

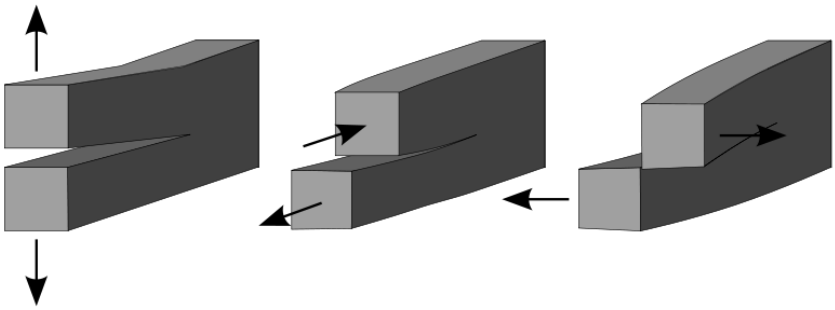

Figure 1 Mode I Opening, Mode II Out-of-plane shear, Mode III In-plane shear

- To simulate Mode I crack propagation, the standard specimen Double Cantilever Beam is used.
- To simulate Mode II crack propagation, standard specimen End-Notched Flexure is used.

The modes are related by a total strain energy release rate $G = G_I + G_{II} + G_{III}$ where $G_I$is energy release rate for mode I, G_{II} for mode II and G_{III} for mode III.

2.2.1 Area Method

As referred to by Carlsson and Pipes [4], Whitney's area method describes how to calculate energy released by finding the area encircled by a load curve.

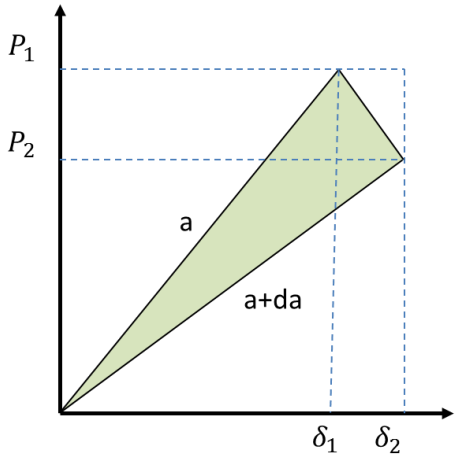

Figure 2: Area method principle

Total released energy can be measured by the area between a force-displacement curve at crack initiation a and force-displacement curve at crack propagation a+da. For linear elastic behaviour, we get the equation

$$dU = \frac{P_1\delta_2}{2} - \frac{P_2\delta_1}{2} \tag{2.3}$$

Where dU is the total energy released. From this we may calculate the strain energy release rate

$$G = \frac{P_1\delta_2 - P_2\delta_1}{2w \cdot da} \tag{2.4}$$

And may calculate critical energy release rate

2.2.2 Compliance Calibration Method

As explained by Kinloch and Young [5], total strain energy may also be expressed by load and beam compliance as

$$U = \frac{1}{2} CP^2 \tag{2.5}$$

Critical value of $G = G_c$, at which point the material at crack tip yields to the plastic strain, can be found by measuring critical load, P_c, at crack length a_c, when crack propagation occurs.

$$G_c = \frac{P_c^2}{2} \frac{dC}{da} \quad , a = a_c \tag{2.6}$$

To derive equation (2.6) a general formula for compliance is found. Different sources such as Carlsson and Pipes [4] derive these from beam theory. However, from earlier tests conducted by Sinnerud [6] and Andreasen and Echtermeyer [7] it was found that this often does not describe the real compliance accurately and an equation is assumed of the form

$$C = \alpha + \beta a^3 \tag{2.7}$$

Where constants α and β are found by curve fitting of test values. Insert (2.7) into (2.6), derive over area and we get the expression of Russel and Street [8]

$$G_{IIc} = \frac{3P_c^2}{2w} \beta a^2 \frac{C}{\alpha + \beta a^3} \tag{2.8}$$

Here C is the measured compliance of the specimen with corresponding crack length. Strain energy release rate may then be calculated from the four parameters crack initiation load, P_c, displacement, δ, width w, and critical crack length a_c.

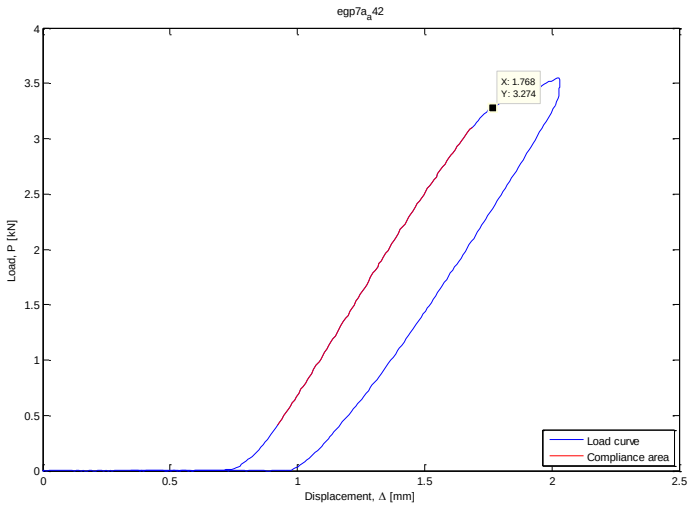

Figure 3: Compliance measuring. Regression fitted to red area.

Compliance is measured using linear regression on an increasing interval, avoiding the viscoelastic area at bottom and peak, of a displacement-load curve. Compliance curve from equation (2.7) is mapped using regression analysis on compliance – crack length data in Sigmaplot with cubic polynomial function $f = y_0 + ax + bx^2 + cx^3$ where a and b are constrained to 0.

2.3 Test procedure

2.3.1 DCB

Each specimen is aligned to avoid torsion stresses, then clamped into grips. It then undergoes a set of loading cycles for measures of load-displacement and crack length. Cycles were conducted with displacement controlled loading set to increase by 2 *mm/s* and to stop at a number above expected critical displacement. At delamination onset, the displacement was stopped, crack tip and crack number was marked on both sides of specimen for later measuring. The specimen was then unloaded at a rate of 10 *mm/s* until approximately zero load. For longer crack lengths, loading rate was increased to 4*mm/s* as load resolution increases with compliance.

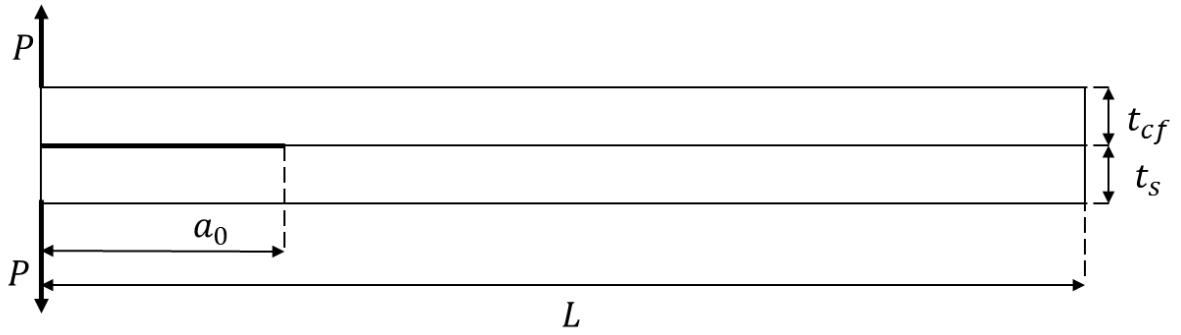

Crack lengths were measured on both sides of specimen and the average length used for calculations. According to ASTM D5528, difference in crack length on both sides should be less than 2 mm. Larger difference could be a symptom of asymmetrical loading

Initial crack length a_0, crack growth length increments $a = a_0 + da$ and the corresponding force P and displacement δ.

Using a leg thickness of 5 mm, zone of damage or nonlinear deformation at delamination front is small relative to the thickness and linear elastic behaviour should occur. [9]

A slow, stable crack development is desired in order to exclude the consideration of dynamic effects. Typically, rapid crack growth is a result of too thick insert or insert that has not been disbanded. To avoid this effect, on the first cycle the specimen is unloaded shortly after initial crack onset. This way, we create a natural Mode I pre-crack [9]. This first cycle is not included in energy release rate calculations.

Displacement control is preferred for stable crack growth. A set displacement creates stresses exceeding critical stress intensity. As fracture begins, the stresses at crack tip will diminish, naturally stopping crack propagation at a new equilibrium. Specimen is unloaded to verify crack closure, with displacement going back to zero implying elastic extrinsic behaviour.

2.3.2 ENF

ENF is a three-point bending of a specimen with a through width crack in longitudinal direction. The stress difference caused by the bending moment below and above causes shear stresses in the bondline.

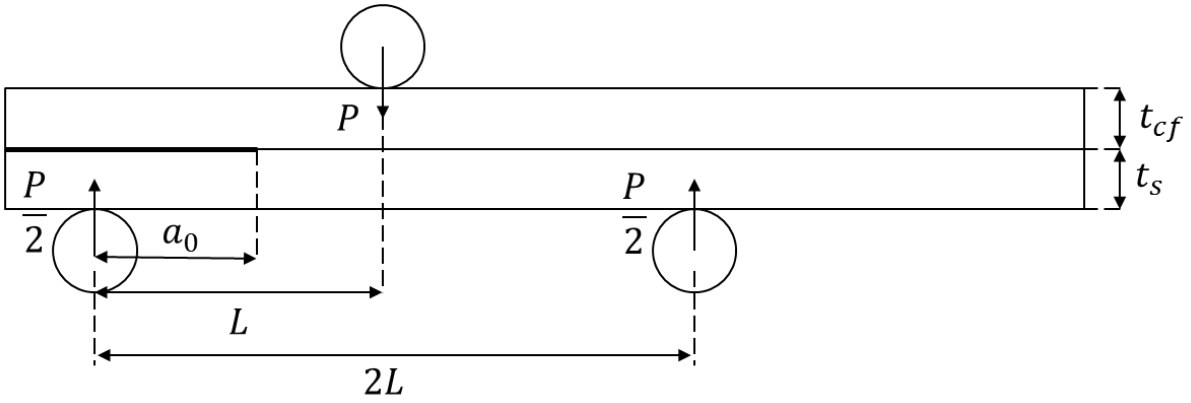

Figure 4: ENF concept

In these tests, span length of $2L = 120\ mm$ is used. Roller diameters are 10 mm. These are parameters used previously by Sinnerud [6], Andresen and Echtermeyer [7]. As the latter also discovered, area method may not be used due to crack arresting at unloading of specimen [7]. Instead the compliance method is used, two compliance calibrations were proposed. For comparison, both were used. One was finding the compliance by recording low-load bending at different crack lengths, as suggested by Andreas Echtermeyer. Another, described in ASTM standard recommendation, was finding compliance at $a = a_0 \pm 10\ mm$ for each specimen tested at a crack length a_0. Compliance would also be measured for a_0 giving a three point curve fit.

Davidson and Teller [10] also conclude that crack lengths should be in the range $0.52 < a/L < 0.7$ while Carlsson and Pipes [4] argue that crack length should be $a \geq 0.7L$ based on beam theory calculation. However, these calculations were not done using a bimaterial specimen and may be less valid in this case. Tests were thus conducted at crack lengths ranging from 17mm - 42 mm with 5 mm interval.

Specimen is loaded at *2 mm/min* until visual crack onset, new crack tip is marked on both sides and then unloaded. Critical load is determined by visual onset.

2.3.3 DCB Fatigue

Following ASTM standard for DCB fatigue tests [11], the specimen are the same as for quasi-static tests. The specimen are cycled between a minimum and maximum displacement $\delta_{min}$and δ_{max}. At onset of delamination growth, the number of displacement cycles N_a is recorded. Onset is determined, not visually, but by 1% increase in compliance, which is approximately 1% decrease in load. Displacement is chosen so that $G_{Imax} = 50\%G_{Ic}$. This is obtained from $\frac{\delta_{\max}^2}{[\delta_{cr}]_{av}^2} = \frac{G_{Imax}}{G_{IC}} = 0.5$ where $[\delta_{cr}]_{av}$ is the average value determined from quasi-static tests. Testing should be done at the same frequency to avoid different heat generation. Recommended values are between *1 Hz – 10 Hz*

2.3.4 ENF Fatigue

No standard is made for ENF fatigue, but the data reduction for ENF is also compliance calibration method and quasi-static tests from the same batch are conducted. For these reasons, the same procedure is used for the ENF subjected to cyclic displacement.

2.3.5 Apparatus

For testing, an Instron 8800 10 kN machine is used. Displacement is measured by crosshead travel, load is measured by a calibrated load cell in upper grips and an SMX 150 USB2.0 camera is used as aid to visually determine crack tip.

3 Specimen production

3.1 Specimen geometry

In order to have the same reference geometry, both DCB and ENF specimen were produced with the same dimensions. ASTM D5528 specifies that specimen must be longer than 125 mm and of width between 20 to 25 mm. For initial crack, a 0.13 mm thick teflon insert is placed onto the steel plate from the end of the specimen to a crack length of $a_0 = 50\ mm$. Normally thickness of arms should range from 3 mm to 5 mm. As high fracture toughness is expected, and a steel thickness of 5 mm is chosen to reduce specimen deflection. Testing done previously by Sinnerud [6] with similar carbon fibre used a ply count of 16 carbon fibre plies of 0.3 mm thickness to maintain similar stiffness as the steel. This gives a slenderness ratio of 25 mm which is within limits specified by ASTM [9].

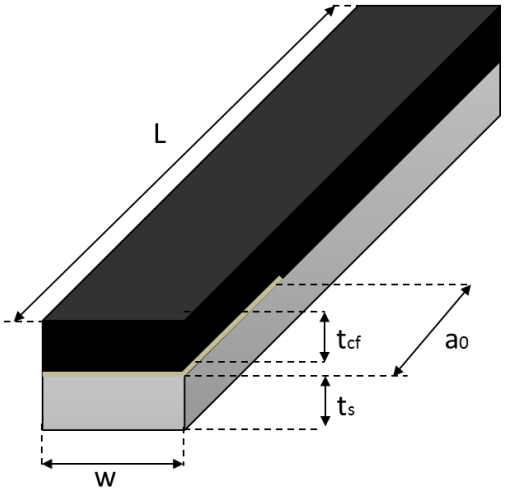

Specimen dimensions	**[mm]**
Length, L	240
Width, w	25
Thickness composite, td	4.8
Thickness steel, ts	5
Initial crack length, a0	50

Difficulties with hinges breaking off in similar testing [6] encouraged the inclusion of a 0.7 mm steel plate insert at 20 mm for later application of mechanical connection further explained in section 3.7.

3.2 Surface treatment

The testing is conducted to compare two surface treatments. Needle scaler and grit blasting. For the CO-Patch project visual assessment of surface should be according to SA 2 ½ [12] and roughness of values 50 < Rz < 85 [13] [7].

3.2.1 Needle scaler

The needle scaler works by pneumatic needles punching the component surface causing plastic deformations in the surface. Scaler used was a Standard Duty Needle Scaler by Ingersoll Rand. The operation was done at approximately 45° angle so as to not beat the debris into the surface. The surface was wiped with a cloth with acetone before and after needle scaler treatment. The surface needed between five and ten wipes of acetone after treatment before wipes showed little to no trace of surface debris/stains.

3.2.2 Grit blasting

Grit blasting was done at Asbjørn Krogstad AS. This is an abrasive blasting method using sand as a medium. Roughness testing was done with an Elcometer 224 to ensure that surface profile meets the SA21/2 standard. Plate 3, 4, 5 and 7 are outside the standard.

Table 1: Plate roughness

	Plate	Mean [µm]	Standard Deviation [µm]	Batch
Grit blasted	**6**	54,2	9,2	ENF-GC
	5	42,9	10,8	DCB-GC
	4	26,1	12,9	ENF-GC-C
	3	33,8	5,8	DCB-GC-C
	2	59,5	8,3	DCB-GP
	1	58,6	11,1	ENF-GP
Needle blasted	**10**	53,8	26,4	DCB-NP
	9	67,5	22,6	ENF-NP
	8	75,6	33,5	ENF-NC
	7	48,7	13,3	DCB-NC

3.2.3 Surface cleanliness

As specified in ISO 8501 [14] , surface was cleaned with wipes of acetone within 15 minutes before commencing layup process.

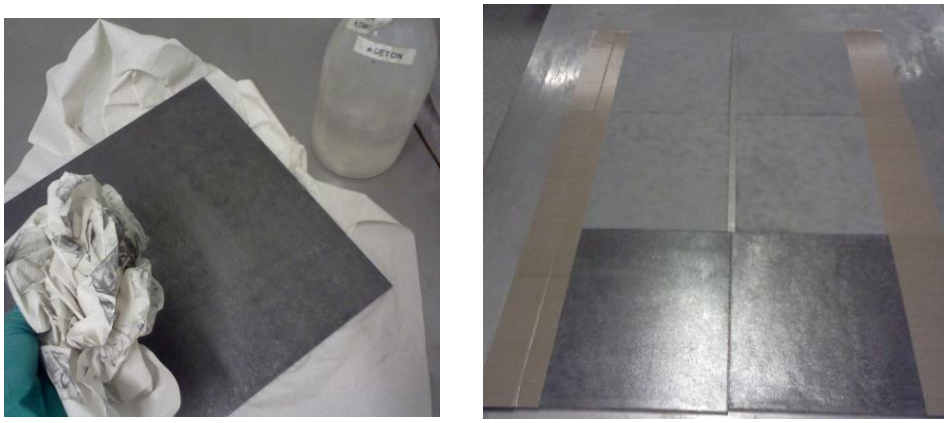

Figure 5: Surface cleaning after needle scaler. Needle scaled surface (bottom) is glossy and dark compared to grit blasted (top).

3.3 Layup

All specimens consist of carbon fibre layer, glass fibre layer, steel layer and a teflon insert. DCB specimen also included a steel insert at layup removed after curing and cutting of specimen.

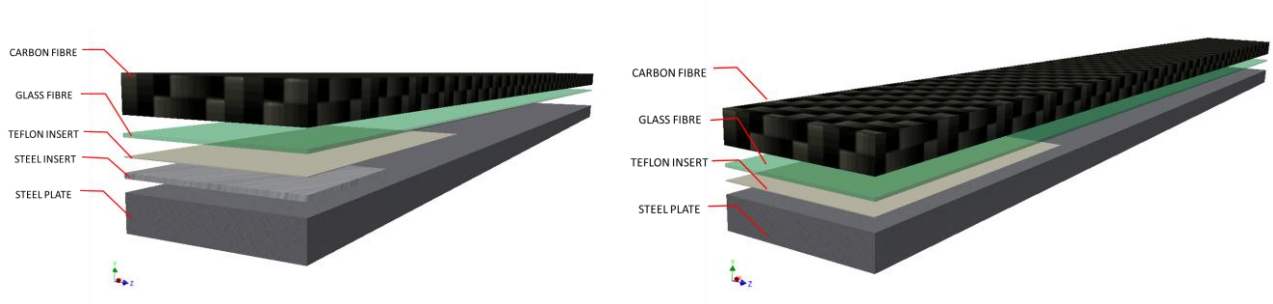

Figure 6: Geometry DCB and ENF

3.3.1 Glass fibre

Galvanic corrosion of steel operating in marine environment can be aggrevated by direct contact between steel and carbon fibre. We thus apply a layer of glass fibre between the patch and the steel. The adhesive interface will be between this layer and the steel as this was shown to be the weakest interface in tests conducted by Echtermeyer and Andresen [7]. Interface strength therefore depends significantly on selection of glass fibre/epoxy system.

Tests were made with two application procedures. Six batches of specimen were made using a ply of $\pm 45°$ stitched glass fibre and Epokite epoxy system applied by brush at 37% moisture and 21°C. This was then cured with peel ply, release film and breather under vacuum, at room temperature for 24 hours.

Four batches of specimen were made using a layer of 0°/90° glass fibre weave, RE295, pre-impregnated with resin SE84LV from Gurit applied to the steel in the same process as application of carbon fibre pre-pregs. This was done at 35% moisture and 23°C.

Pictures of bondline are shown in

Figure 31 and Figure 33 in the appendix.

3.3.2 Carbon fibre

Carbon fibre was applied as cut out sheets of unidirectional pre-pregs. Test laminates must contain an even number of plies and yield same stiffness as steel part. [9] 16 plies of dimensions 250mm x 250 mm x 0.3 mm were laid in longitudinal length. On the top, peel ply was applied for smooth structure, pre impregnated to avoid reduction in resin volume of carbon fibre layup. Earlier work done by Sinnerud [6] on similar material found ply thickness to be 0.3 and that a ply count of 16 would render equivalent stiffness to that of a 5 mm thick steel beam.

3.4 Specimen overview

A total of ten batches of test specimen were laminated in one session then cured in two sessions.

Table 2 Batch production

	Precured glass fibre	Pre-preg glass fibre
Needle gun	8x ENF-NC	8x ENF-NP
Grit blasted	8x ENF-GC, 8x ENF-GC-C	8x ENF-GP

	Precured glass fibre	Pre-preg glass fibre
Needle gun	8x DCB-NC	8x DCB-NP
Grit blasted	8x DCB-GC, 8x ENF-GC-C	8x DCB-GP

3.5 Curing

After layup, the adhered patch is placed in an oven for curing. Because the thermometer of the oven records temperature very close to the heat element and regulates heating thereafter, actual temperature is lower. Curing temperature was set to 95 °C for 10 hours and temperature recorded with an independent thermometer at just above specimen height. All tests should undergo the exact same curing, but this was not attainable due to size limitations. Instead, DCB and ENF batches were cured separately as comparison between the two should not be weighted.

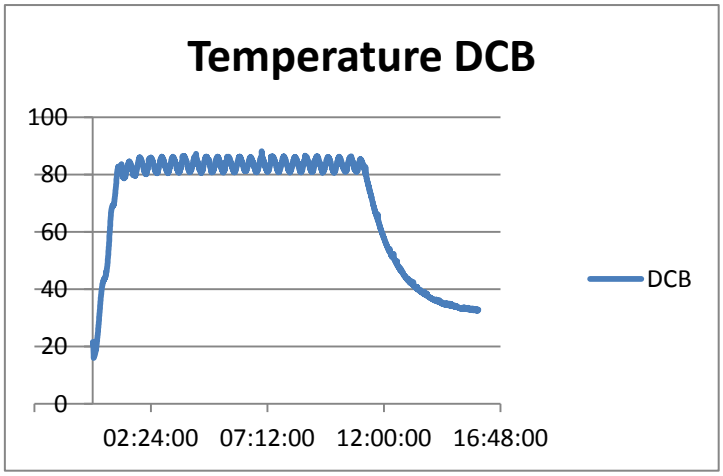

Figure 7 Curing history of DCB batches

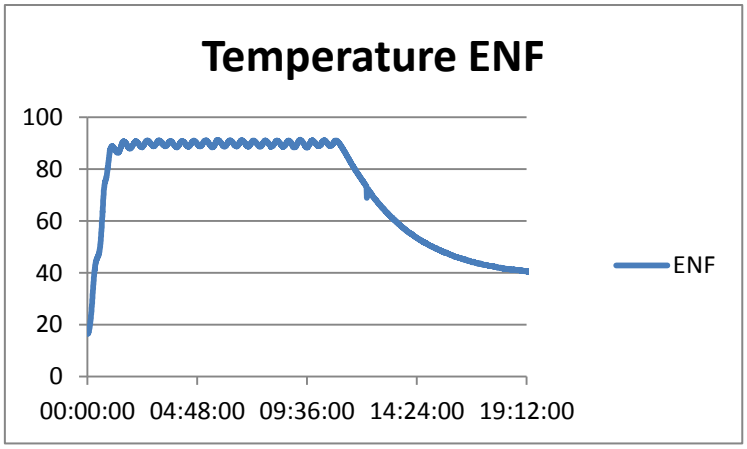

Figure 8 Curing history of ENF batches

Fluctuating temperature curves during curing of the DCB tests can be explained by an open valve. Nevertheless the tests maintained at least 83 degrees over 10 hours. The temperature measurement was made above the valve, the specimen are placed below the valve. This could mean a higher curing temperature than recorded.

After curing the ENF tests, a leak was discovered in the tubes from the pump to the specimen. The vacuum was tested after opening the oven and the pump could produce a 95% vacuum even with the leak. This is above the minimum requirement of 85% vacuum specified by SP Gurit [15]. In addition, vacuum was last checked 6 hours into curing and as this was closer to a 90℃, curing was probably already finished.

Heating speed should be $< 2\ °C/min$. For ENF the average was 1,13 °C/min and for DCB it was 0,94 °C/min.

3.6 Cutting

Specimens were cut from plates with a water jet. This was to avoid the problem of heat development. This results in slightly uneven sides as the jet is deflected differently through steel and carbon fibre.

3.7 Hinge application

According to ASTM D 5528 [9] piano hinges were aligned and adhesively bonded to adherends. In similar tests conducted by Arve Sinnerud adhesive failure occurred between hinges and adherends. Because of this it was decided to insert a steel plate of 0.7 mm thickness covered with release agent between carbon fibre and steel in the layup. This was removed after cutting to leave a gap. In the gap, there is room to place a mechanical fastening. A screw connection between hinge and steel adherend was also used to create a mechanical fastening.

3.8 Material properties

3.8.1 Epoxy

Values gathered from datasheets [15] [16].

Table 3: Adhesive values

[MPa]	E	υ	G
SE 84LV	3280	0.35*	1200
Epikote RIMR 135/RIMH 137	3200	0.35*	1185

*,The υ was taken from [6]

3.8.2 Carbon fiber

The carbon fibers are Toray M46JB pre-impregnated with resin SE84LV from Gurit [15]. All plies are orientated 0° unidirectional to crack direction. As mentioned in section 3.1, Sinnerud [17] used the same resin, but the fibers were Grafil Pyrofil with elastic modulus of 455 GPa whereas Toray M46JB has 445 GPa. The tested values of the Pyrofil are used for modeling and the assumption that 16 plies provide almost equal stiffness to the 5 mm steel.

Table 4: Carbon fiber constants

[GPa]	E_1	E_2	E_3	G_{12}	G_{13}	G_{23}	v_{12}	v_{13}	v_{23}
CF	222.3	15.87	15.87	4.3	4.3	3.4	0.2525	0.2525	0.5

3.8.3 Steel

Average values for steel are used. Differences due to processing are assumed negligible.

Table 5: Steel values

[MPa]	E	υ
Steel	207 000	0.3

4 Experimental results

Test batches DCB-NP and ENF-NP delaminated at adhesive interface between steel and glass fiber layer. This could be explained by the needle scaled surface. Though it showed better roughness values, it was shiny and needed many wipes of acetone before no debris was left. Of the ENF-NC only one specimen completely delaminated, however the others had delaminated at the edges, making it impossible to visually determine crack tip. DCB-NC had the same problem, and delaminated quickly during testing.

Figure 9 Interface of delaminated ENF-NP specimen.

4.1 DCB

First test of DCB GC showed very high critical energies. This could be due to elastic energy used on elongation of hinges, however, high occurrence of fiber bridging is a more likely reason. Long before each crack propagation, sounds of fibers snapping indicates load was spent straining fibers still attached to both adherends causing high load curves.

4.1.1 Area Calculations

Initially the area was calculated using the function *trapz()* in Matlab. This rendered very high values, as shown in Table 6. This could be explained both by load exceeding maximum stress of bridged glass fibers, but could also imply crack pro and the assumption is made that this is because of large non-linear effects and plasticity. Certain curves show considerable plastic strain. An approach was attempted assuming linear elastic behavior as explained in Area Method 2.2.1. This neglects plastic strain and nonlinear behavior, but may introduce uncertainties in selection of crack onset and cause higher scatter.

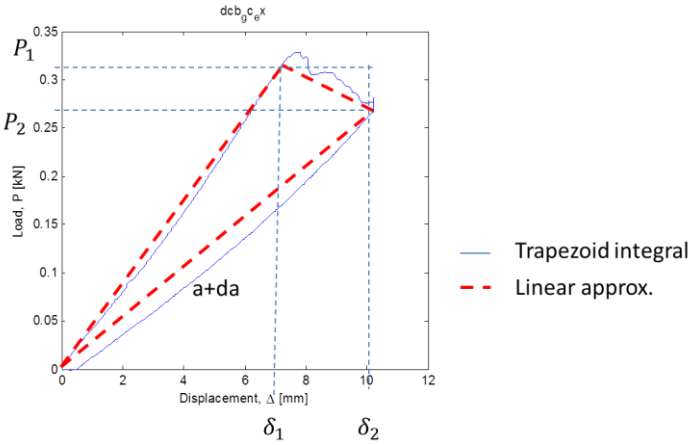

Figure 10 Linear elastic vs. trapezoid integral area calculation approach

Unloading displayed the most elastic behaviour and reference displacement. In strict comparison between the methods, plastic and nonlinear effects may account for 30% of total energy release rate for DCB-GC and 37% for DCB-GP.

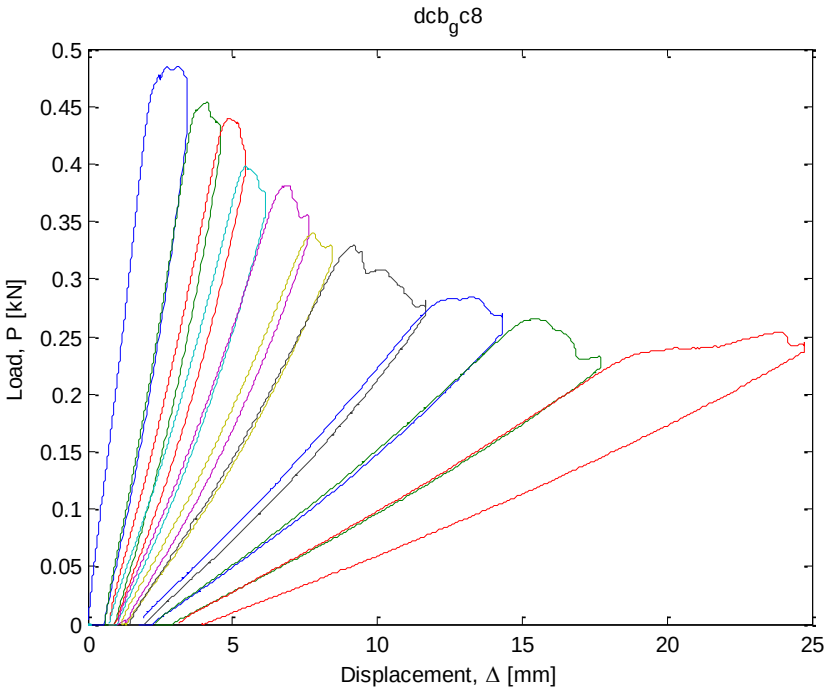

Figure 11 Load curve DCB-GC 8

Initial curves are more subject to permanent displacement. Other than plastic strains in the specimen these could also be the result of plastic strains in the hinges and mechanical fastening.

4.1.2 Mode I Results

All test results are shown in Figure 20 and Figure 21.

Table 6 Comparison Area method calculations

Gic, DCB Area methods						
		# Calc.	Mean, μ	Standard deviation , σ	μ-σ	μ-2σ
DCB-GC	Trapezoid Integral	58	1992,6	463,8	1528,7	1064,9
DCB-GC	Linear Approx.	56	1333,7	431,0	902,8	471,8
DCB-GP	Trapezoid Integral	50	895,6	338,8	556,8	217,9
DCB-GP	Linear Approx.	47	565,5	247,7	317,8	70,1

Values from testing were considerably high compared to similar testing listed by Kinloch and Young [5]. This could be explained by fibre bridging, a typical occurrence in unidirectional DCB testing. The fibres' contribution is considerable, however, as seen in Figure 12, it is apparent that the occurrence is far from homogenous and very conservative values should be used.

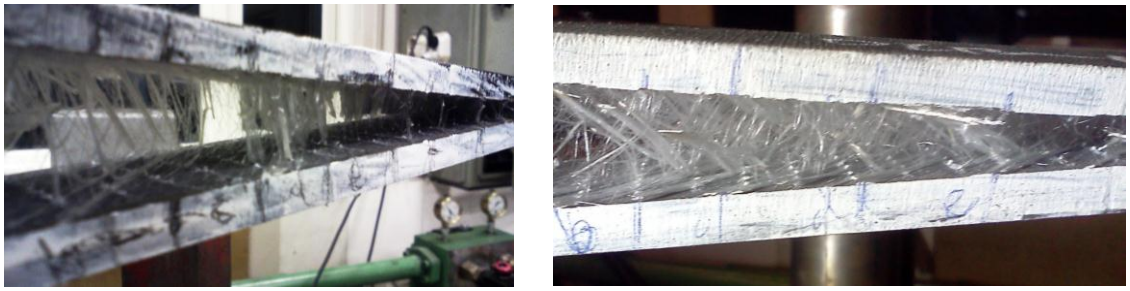

Figure 12 Fibre bridging on DCB-GC-1 (left) and DCB-GC-2 (right)

Only fibres of the bottom layer contributed to the bridging meaning cohesive fracture occurred closer to the steel interface.

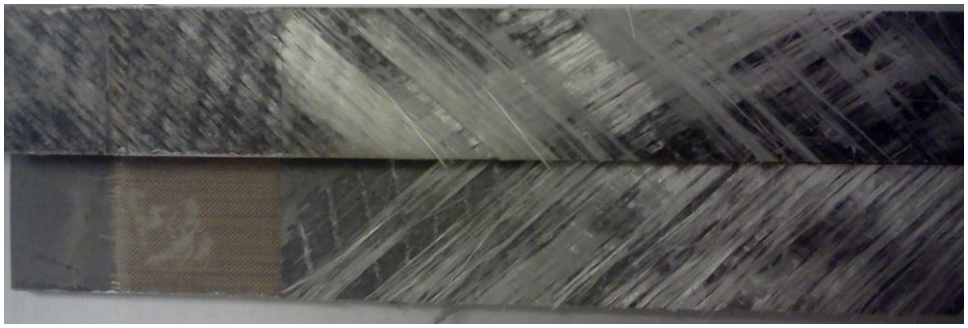

Figure 13 Crack surface DCB-GC-4

The fracture of DCB-GP in Figure 14 showed little or no bridging. The fracture surface contains traces of resin at the middle of the steel, implying a cohesive failure and adhesive failure at the edges.

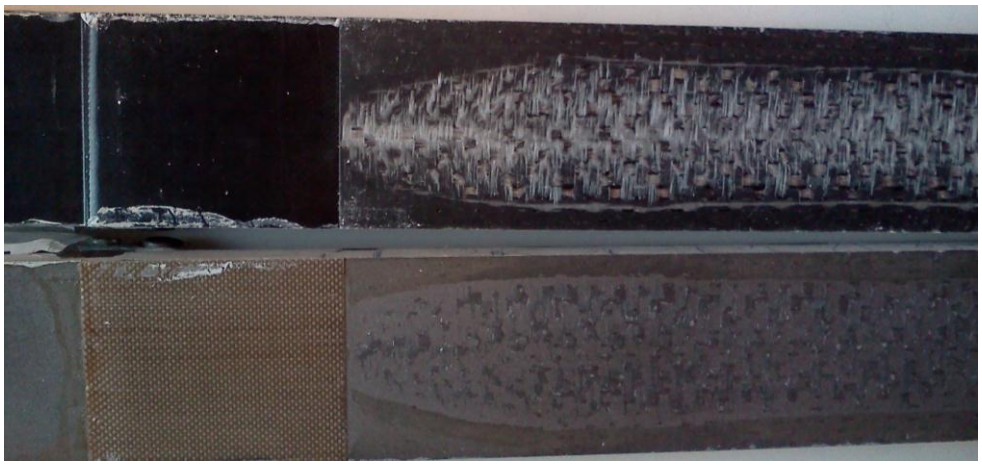

Figure 14 Fracture surface DCB-GP-1

The DCB GP had some occurrences of delamination in the carbon fibre, especially specimen 6. The crack proceeded to develop in the carbon fibre layer parallel to the interface delamination. It was apparent that the load condition had changed and further results were neglected.

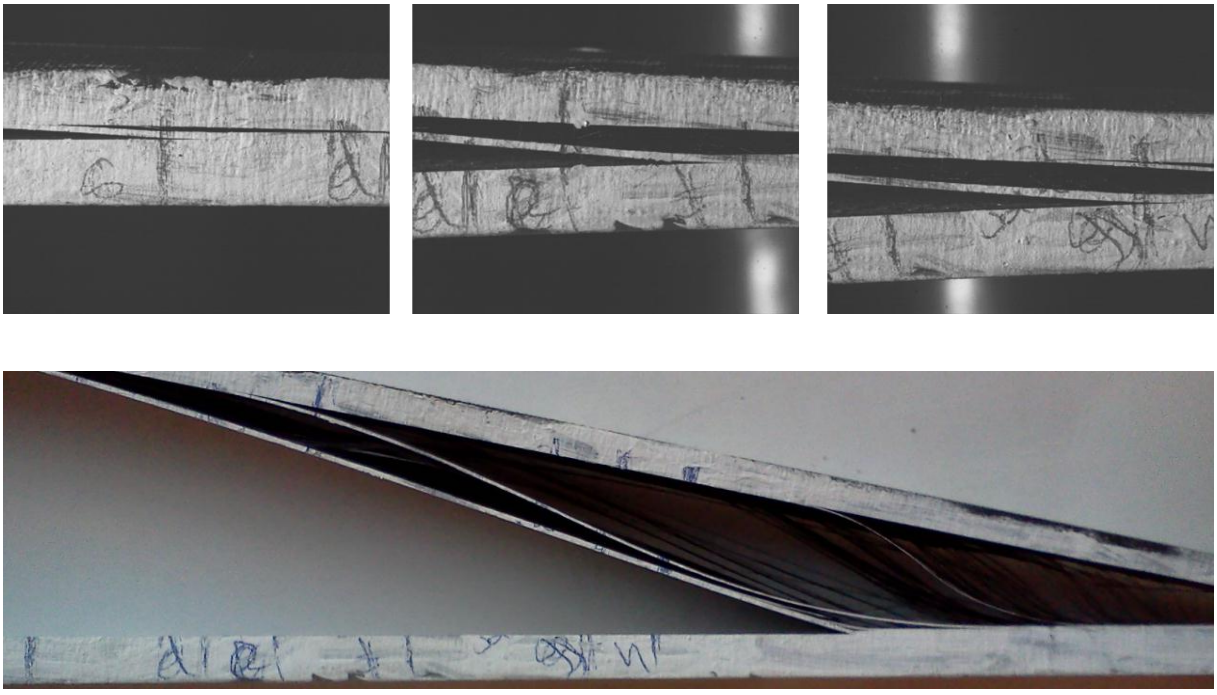

Figure 15: Delamination in carbon fibre layer

4.2 ENF

4.2.1 Compliance Calculations

Trials were done using both a 3-point calibration of each specimen tested at a certain crack length, and an 8-point calibration on the first and second specimen done for all relevant crack sizes. The results show significant differences as in Figure 16

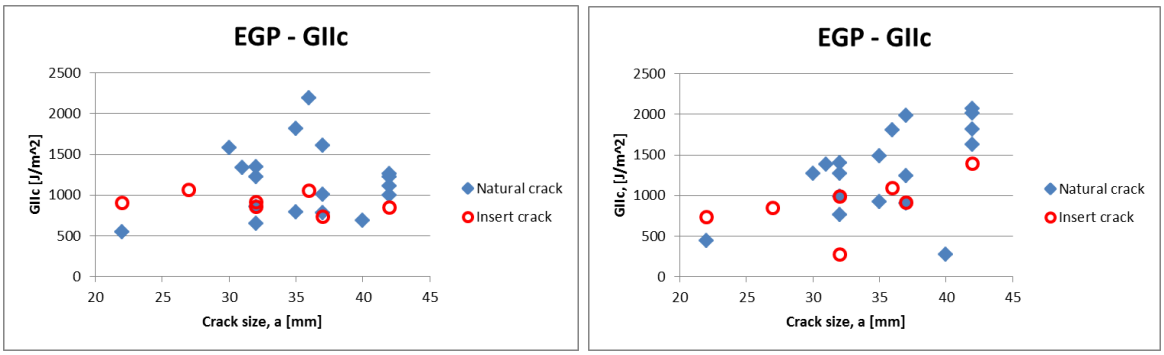

3 point $\mu = 1105,\ \sigma = 373$ 8 point $\mu = 1103,\ \sigma = 572$

Figure 16: Compliance calibration comparison

These have not been fitted with the measured compliances from the tests and tests show that, as the crack propagates, it may give different compliances for the same crack length. To compensate for this, a curve fit was done on all compliances measured. This was used for final G_{IIC} calculations. The combined curve fit produced the constants in Table 7.

Table 7: Compliance constants

Constants	ENF-GP	ENF-GC
α [mm/kN]	0,19	0,20
β [mm^{-2}/kN]	1,3E-06	1,0E-6

Inserted cracks are plotted separately to note whether there is a significant effect. The blunt distribution seems fairly random and crack tip at initial crack does not seem to have any significant effect in ENF testing.

4.2.2 Mode II Results

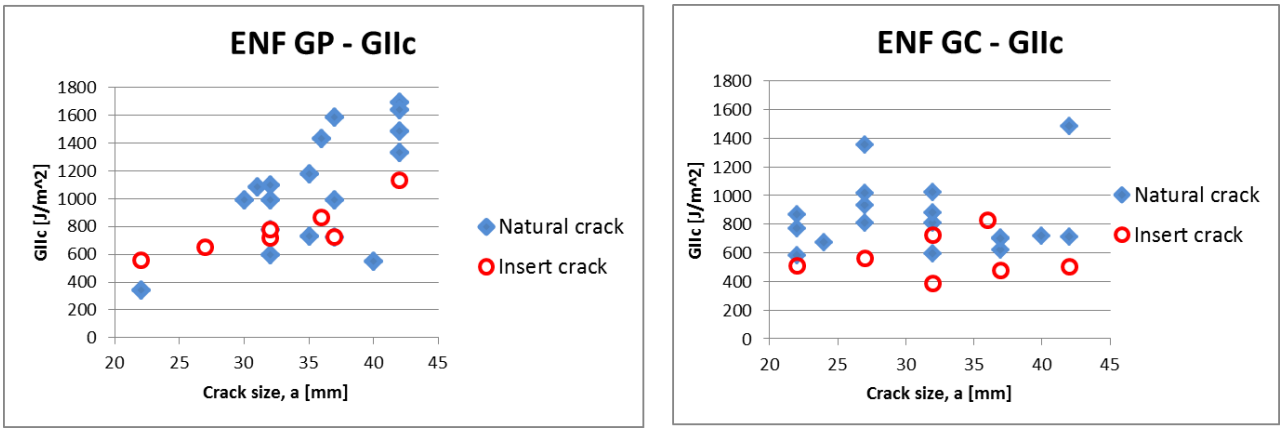

Figure 17: GIIc vs. crack length

Values using the combined curve also have a significant scatter caused by crack length dependency. In Figure 18 average energy release rate for the different crack lengths was plotted. Looking at the distribution of strain energy release rates over crack length, we see that the dependency is higher for the ENF-GP. Comparison should be made separately.

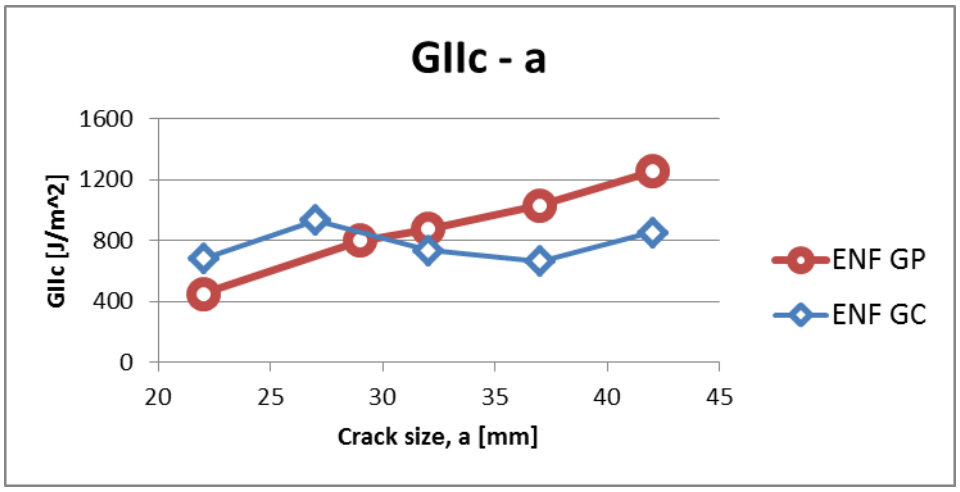

Figure 18: Energy release rate – crack length dependency for ENF

Figure 18 insinuates ENF GP to be more dependent on crack size. Nevertheless, for comparison, mean energy release rate for the two application methods is found for crack sizes within a span of $22 \leq a \leq 42$.

Table 8 ENF Comparison

GIIc [J/m^2], aϵ[22,42]					
Batch	# Tests	Mean, μ	Standard deviation, σ	μ -σ	μ -2σ
ENF-GC	25	769	255	204	170
ENF-GP	26	982	361	199	155

Table 8 shows a small difference in energy release rate between the two. The pre-impregnated glass fibre shows a slightly higher value

5 Simulation

A simulation was made in Abaqus (6.10-2) to extract the properties of the interface and to test the laws and settings needed for a good replication so that these may be used for strength analysis of other structures.

5.1 Fracture modelling

In Abaqus one can model cohesive contact either with surface-based cohesive behaviour, virtual crack closure, VCCT or with cohesive zone modelling, CZM. VCCT is assumes the energy released at delamination is equal to the work required to close the crack. Difficulties occur for VCCT when simulating progressive delamination. CZM uses cohesive elements and may predict both onset and propagation of delamination. [18] CZM is the method mainly used for adhesive joints and delamination problems. As both adhesive and cohesive failure is possible in the crack propagation, this analysis will use cohesive elements.

5.1.1 Cohesive Zone Modelling

One way of modelling cracks is to use Cohesive Zone Modelling which describes the cohesive zone as the integral of the restraining stresses, dependant on separation distance.

Cohesive zone modelling uses this traction-separation law to simulate progressive delamination.

Modeling fracture with cohesive elements must include three behaviors:

- Elastic behavior
- Damage initiation
- Damage evolution

For the elastic behavior it is necessary to determine the penalty stiffness coefficients K_{nn} for normal stresses and K_{tt} for shear. It is assumed out-of-plane and in-plane shear are equal.

By this law delamination growth occurs as long as the total energy release rate G is greater or equal to the critical value G_C. The mix ratio of normal and shear values must be considered. In Abaqus it is implemented three ways to account for this. BK, tabular or power law.

5.1.2 Penalty stiffness

A high penalty stiffness must be chosen for rigid connection between adherends and not introduce compliance from the cohesive elements. However, an overly high value may lead to oscillations and difficulties in convergence. The formula presented by Turon was attempted define penalty stiffness [18]

$$K_i = \alpha \frac{E_i}{t} \tag{5.1}$$

Here $\propto \gg 1$ typically 50, however this should be regulated with element size. Penalty stiffness corresponds to modular stiffness of similar direction. For this, the elastic modulus of the adhesive material, Epotik, was used. This overestimated the load by a twofold. Many iterations were attempted changing other parameters like mesh density and interface strength while either getting too high results, or no convergence. A different formula referred to in a report by Simulia [19] was presented by T. Diehl as

$$K_i = \frac{2G_i}{\delta_{ratio}\left(\delta_f\right)^2} \tag{5.2}$$

Here δ_{ratio} is usually set to 0.5 and δ_f is displacement at failure, a problem dependent parameter typically 5% of cohesive element length.

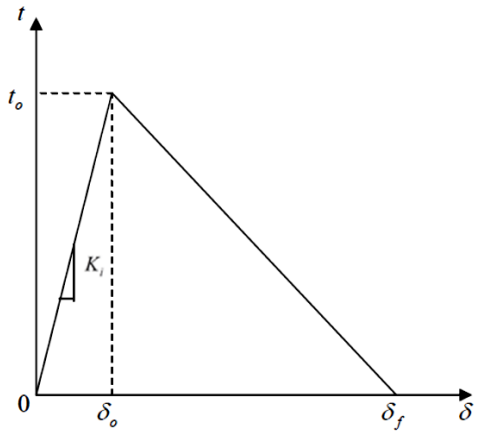

Figure 19 Stiffness in relation to traction-separation [19]

5.1.3 Damage behavior

For damage initiation, the interface yield strength S_n in tensile direction and $S_{tt} = S_{tt}$ in shear direction must be determined. For damage evolution the critical fracture energies are G_{IC} for normal mode and G_{IIC} for shear mode first direction and second direction.

Although data is given by both epoxy distributors on shear strength, the interface strength will most likely differ. A proposed way of calculating interface strength is

$$S_i = \frac{2G_i}{\delta_f} \tag{5.3}$$

Song [20] argues that tabulated BK ratio yields most correct simulation. With this option, the material parameter η proposed that it is to be found by least square curve fit of equation (5.1) using values from experimental data.

$$G_C = G_{IC} + \left(G_{IIC} - G_{IC}\right)\left(\frac{G_{shear}}{G_T}\right)^{\eta} \tag{5.1}$$

Initially, this will be subjected to trial and error.

5.1.4 Mesh density

Cohesive zone length is the area behind the crack which is subject to strain and possible plasticizing. In Abaqus this corresponds to amount of cohesive elements in the span of one structural element. This has been shown to be a material property following the formula by Turon [18]

$$l_{cz\_i} = \left[E_2 \frac{G_{iC}}{S_i^2}\right]^{1/4} h^{3/4} \tag{5.2}$$

Here E_2 is the transverse Young's modulus while S_i is interface strength and h is the thickness of the substrate. This formula may be used provided that the interface strengths are

known. Turon concludes that no more than 5 elements are needed for cohesive elements smaller than 0,25mm and states that a reasonable assumption is to use 3-5 cohesive elements over the span of one structural element. In this analysis, smaller cohesive element size than 2 mm rendered difficulties in convergence, and solid element size was set to 5 mm.

Once the damage initiation criterion of the cohesive element is satisfied, the stiffness of the element is degraded according to Equation 8. This represents the softening response of the cohesive element

$$t_i = (1-d) K_i \delta_i \tag{5.3}$$

Where t is traction, d is the damage variable, which has the value d = 0 when the interface is undamaged, and the value d = 1 when the interface is fully fractured. Fully degraded elements can take zero stress and are deleted.

Cohesive elements can be bound to the solid elements either by use of tie constraints or shared nodes. In this analysis tie constraints are used.

5.1.5 Viscous regularization

The kinematic modeling of crack growth may result in singularity-problems with residue stresses. A viscous regularization factor was included for reduction of singularity problems. This was set to 1e-5 as used by Simulia [19].

5.1.6 Boundary conditions

Boundary conditions were as shown below. Load was introduced by a reference point constrained with a kinematic coupling to the upper left edge.

Figure 20: Boundary conditions DCB

Also in the case of ENF load was applied on reference point with a kinematic coupling to the model.

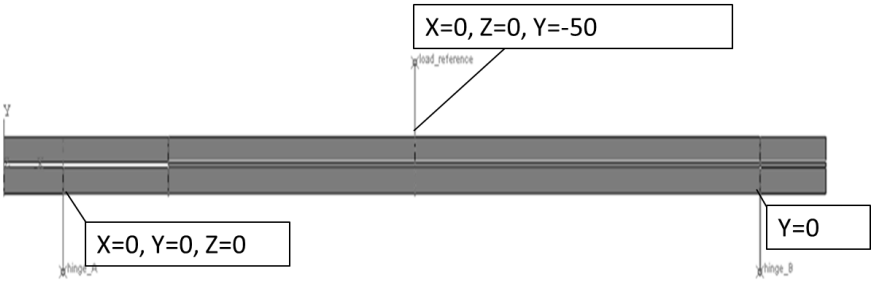

Figure 21: Boundary conditions ENF

This way, only the partitioning needs to be moved in order to change the crack length. Surface to surface contact with hard contact property was applied between the opposing surfaces of the two beams.

5.2 Solid modelling

For correct compliance and stress transfer it is important that the structural parts resemble the real specimen. For the carbon fibre, a homogenous layup was assumed as it only consists of 0° plies and no stresses will be extracted. Values were imported from section 3.8. The solid elements are cubic with 20 nodes and reduced integration, C3D20R. This makes for quadratic displacement function which is important when modelling flexure in thin structures.

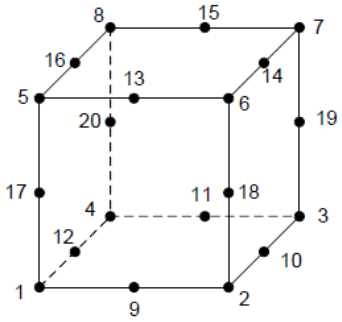

Figure 22: C3D20R element for structural modeling

5.3 Results and comparison

In the ENF model, problems with the stiffness of the cohesive elements caused problems getting useful results. The use of Diehl's equation for penalty stiffness (5.2) rendered results, however initial elements were eliminated in the first increment and loads were not in the same magnitude with 150 N compared to the forces measured during testing of 2-5 kN. With cohesive element size reduced to 1 mm, stiffness was increased, but convergence failed at a load of 300 N and before fracture was achieved. The time limit made no more optimizing iterations possible.

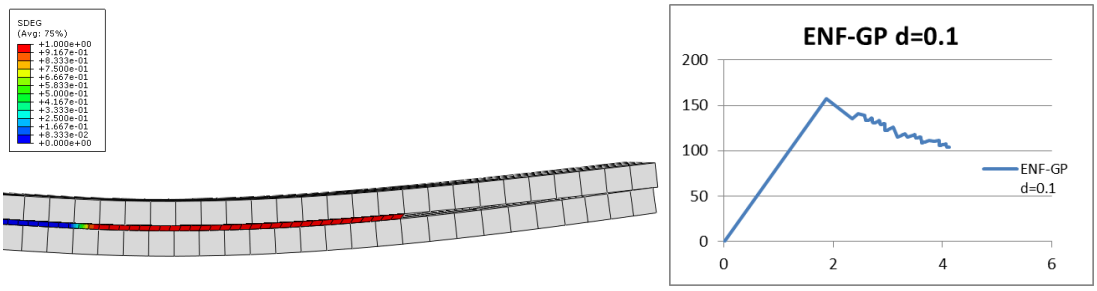

Figure 23: ENF-GP model and corresponding load curve

As shown in Figure 23, cohesive elements at crack initial crack have failed at first increment and crack propagation is continuing beyond load point.

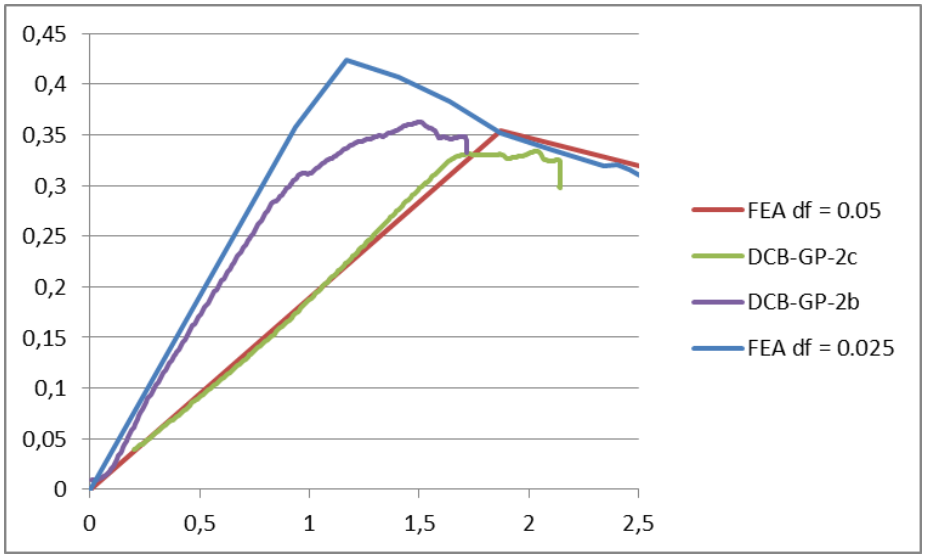

Figure 24: Comparison of numerical and test results for DCB-GP-2

Figure 24 shows example of how stiffness and strength changes by only altering one parameter δ_f including reference curves from test results. Crack lengths of test results are longer than crack length for element model. Matching stiffness would therefore not be correct.

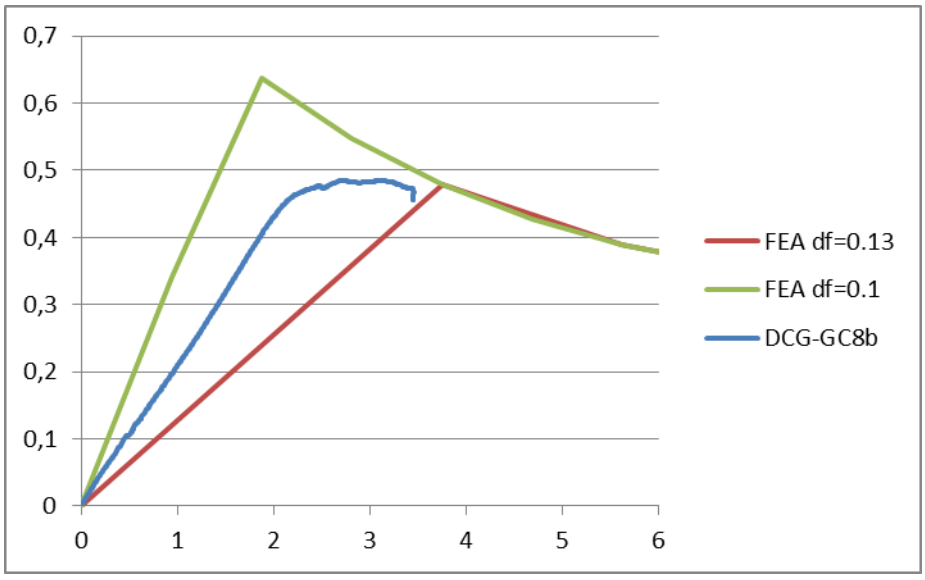

Figure 25: Comparison of numerical and test results for DCB-GC-8

This simulation was made as a test to find a good modeling procedure. Figure 24 and Figure 25 show good potential even though precise fit was not acquired. A fit should be trivial in this case, however the crack length is not the same for crack *b* and the model. Damage evolution is not as well modeled. The mix ratio BK power η showed little significance when tested. This could be due to the actual absence of other fracture modes.

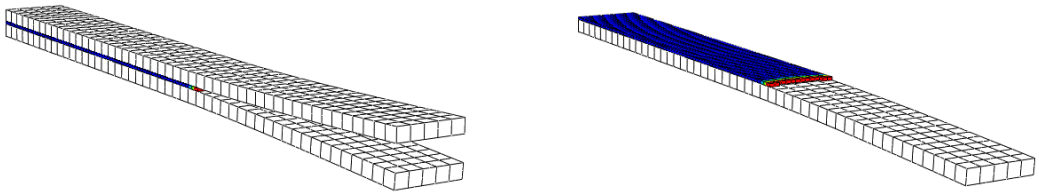

Figure 26: Degradation in the DCB simulation. Crack shows a thumbnail pattern.

Unloading was not considered, hence it is not represented in comparisons.

6 Discussion

For the DCB GC results were very high, most likely due to the high density of fiber bridging. In the case of DCB GP, cohesive failure was only present at the middle of the crack tip and fibers were not ripped and left on both surfaces rather there had seemed to occur interface failure between fibers and matrix. The pre-impregnated glass fibers were weaved meaning they could not move as much relative to each other. This could contribute to the difference in amount of bridging.

The fact that the loads were so high in DCB testing introduces problems of plasticity and significant deformations in extrinsic components such as hinges, screws, fastening, grips or testing machine. These factors may have contributed to the high scatter which suggest that the values should be interpreted with care.

The delamination of needle scaled batches implies that it is not an optimal surface treatment. However, more research should be done into cleaning methods and correct use, before writing it off completely. Steam cleaning or acetone bath of surface could be alternatives to cleaning beforehand.

Both the 3 point calibration and the 8 point calibration showed local deviations when compared to the measured compliance during tests. This could be due local differences along the specimen, uneven crack propagation or plastic deformations causing different compliance calculations when cracks are of equal length. A curve fit including these measures would find the compliance curve which renders the least scatter in total for all specimens, however, the scatter from different measurements at equal crack lengths will not be removed. Individual compliance curves for each crack increment done by three point calibration should have a positive impact on scatter.

In the simulation, a finer mesh would be desirable, but caused convergence errors when Diehl stiffness was used. This could be a result of the large specimen geometry. Other affecting parameters such as viscous regularization could be attempted changed.

7 Conclusion

Cleaning of needle scaled surface using only wipes of acetone is not sufficient. Grit blasting showed good bonding properties.

Glass fiber applied in wet layup showed very high energy release rate in mode I testing and high occurrence of fiber bridging. Though the actual contribution remains unknown, fiber bridging definitely had an effect on the load curves obtained. When testing for high interface strength, all other factors should be dimensioned accordingly to avoid extrinsic effects on load curves.

ENF-GP and ENF-GC showed little difference in mode II energy release rate. They showed different dependency on crack length. No pattern was found in difference between inserted and natural crack energies.

Compliance calibration should include all compliance values. Preferably compliance calibration should account for differences in compliance when crack lengths are seemingly the same. This may be done by calibrating for each crack increment.

Proposed simulation procedure using cohesive elements proved potential, but had a limited set of iterations to find the proper parameter combinations.

8 Further work

Further testing should be done using thicker or stiffer and stronger hinges, load blocks or with increased specimen slenderness L/h to deny the increase in specimen compliance.

The limits of the needle scaler should be further investigated and the reason determined for early delamination.

Modeling of fatigue behavior using FEA fatigue properties of application procedures that render good quasi-static results should be found.

Comparison to total load curve of a specimen should be carried out, and a better description of damage evolution may be obtained using tabular mixed mode ratio. A subsequent unloading step may render interesting results. Also including plastic deformations to solid elements for analysis of energy released due to plastic strain. Different methods, such as Discrete Cohesive Zone Modeling explained by Xie and Waas [21] and XFEM used by Nagashima, Omoto and Tani [22] may render shorter computation times. This could be useful for modeling of further steps.

The effect of fiber bridging relating to energy release rate, and the reliability of its occurrence could be useful for less conservative dimensioning of relevant materials.

9 Bibliography

[1] "www.adhesives.org," [Online]. Available: http://www.adhesives.org/TrainingEducation/StudentResources/DesignofAdhesiveBonds/MechanicsofAdhesion.aspx.

[2] A. P. D.A. Dillard, Adhesion science and engineering, Elsevier Science Publishers, 2002.

[3] A. Griffith, "The Phenomena of Rupture and Flow in Solids," JSTOR, 1921.

[4] L. A. Carlsson and R. B. Pipes, "Experimental Characterization of Advanced Composite Materials," Prentice-Hall, Inc., 1987.

[5] A. Kinloch and R. Young, "Fracture Behaviour of Polymers," Elsevier, 1983.

[6] A. Sinnerud, "Adhesion of metal-composite joints," NTNU, 2011.

[7] H. W. Andresen and A. T. Echtermeyer, "Critical energy release rate fr a a CSM reinforced carbon fibre composite/steel bonding," Elsevier, 2005.

[8] A. Russel and K. Street, "Factors affecting the interlaminar fracture of graphite/epoxy laminate," 1982.

[9] "Standard Test Method for Mode I Interlaminar Fracture Toughness of Unidirectional Fiber-Reinforced Polymer Matrix Composites," ASTM International, 2007.

[10] B. D. Davidson and S. S. Teller, "Recommendations for an ASTM Standardized Test for Determining GIIc of Unidirectional Laminated Polymeric Matrix Composites," ASTM International, 2010.

[11] "Standard Test Method for Mode I Fatigue Delamination Growth Onset of Unidirectional Fiber-Reinforced Polymer Matrix Composites," ASTM International, 2004.

[12] N. Standard, "M-501 Surface preparation and protective coating," www.standard.no, 2004.

[13] "ISO 8503 Preperation of steel substrates before application of paints and related products," Internation Standards Organization, 1996.

[14] "ISO 8501 Preperation of steel substrates before application of paints and related products," International Standard Organization, 1996.

[15] "SE 84LV - Low Temp Epoxy Prepreg System (v12)," SP Gurit, 2010.

[16] Momentive, "EPIKOTE Resin MGS RIMR 135 and EPIKURE Curing Agent MGS RIMH 134–RIMH 137," 2006.

[17] A. Sinnerud, "Adhesion of metal-composite joints," 2010.

[18] A. Turon, C. Dávila, P. Camanho and J. Costa, "An engineering solution for mesh size effects in the simulation of delamination using cohesive zone models," Engineering Fracture Mechanics 74, 2007.

[19] Dassault Systemes Simulia Corp., "Selecting Material Parameters for Cohesive Elements Defined in Terms of Traction-Seperation".

[20] K. Song, C. Dávila and C. A. Rose, “Guidelines and Parameter Selection for the Simulation of Progressive Delamination,” SIMULIA, 2008.

[21] A. M. W. De Xie, “Discrete cohesive zone model for ixed-mode fracture using finite element analysis,” Elseiver, 2006.

[22] G. S. S. Lâaszlâo P. Kollâar, Mechanics of Composite Structures, Cambridge University Press, 2003.

[23] D. Roylance, “Introduction to Fracture Mechanics,” Massachusetts Institute of Technology, Cambrigde, MA, 2001.

[24] Y. O. S. T. Toshio Nagashima, “Stress intensity factor analysis of interface cracks using X-FEM,” John Wiley & Sons, 2003.

[25] Sun, B. D. Davidson and Xuekun, “Geometry and Data Reduction Recommendations for a Standardized End Notch Flexure Test for Unidirectional Composites,” ASTM International, 2006.

A.1 Test results

Test results

Table 9 DCB GP, Linear approximation

#	Specimen	Crack iteration											
	b	c	d	e	f	g	h	i	j	k	l	Mean	STDV
1	607,9	319,3	375,2	519,1	457,1	609,9	533,3	491,7	562,4	420,0		489,6	96,9
2	189,6	271,3	432,7	278,0	384,7	417,2	520,1	577,6				383,9	131,6
3		354,1	309,0	706,4	389,1	427,1	477,0	478,5	832,4			496,7	181,0
4		477,0	556,9	338,6	596,8	652,2						524,3	121,9
5	203,3	282,4	968,3	558,4	1258,2	772,8	730,9	971,7	916,1	704,9	894,0	751,0	309,9
6		378,0	601,3	917,3	342,9	934,4	1144,8					719,8	328,2

Table 10: DCB GC, Linear approximation

#	Specimen	Crack iteration											
	b	c	d	e	f	g	h	i	j	k	l	Mean	STDV
1	1246,1	1295,7	1215,3	2504,9	1487,3	1022,3						1565,5	627,2
2	908,1	1030,8	1064,4	1663,5	1266,5	1310,6	2501,7					1392,2	547,6
3		910,2	1237,1	1947,8	1265,0	1591,5	1143,0	1784,0	1215,7			1386,8	352,0
4	547,4	1423,7	1561,4	1067,5	1617,0	2205,2	1510,3	1272,8	2062,0	1775,936		1504,3	478,3
5		850,6	1180,0	1136,8	1884,6	1391,6	1984,0	1931,4				1203,9	453,4
6		872,3	907,0	1086,5	1001,5	1230,3	1241,0	1037,9	1024,8	1134,713	1682,07	1121,8	231,1

A.2 ENF GC

Table 11: ENF-GC

Specimen	# Crack	a	GIIc
1	a	36	825,15
	b	32	591,90
	c	27	805,04
	d	24	673,30
2	a	32	387,71
	b	40	717,09
3	a	22	508,72
	b	22	582,77
	c	22	767,16
	d	22	868,51
4	a	27	564,09
	b	27	933,76
	c	27	1017,37
	d	27	1354,51
5	a	32	724,92
	b	32	807,96
	c	32	880,87
	d	32	1020,17
6	a	37	477,73
	b	37	622,86
	c	37	706,08
	d	37	694,73
7	a	42	501,94
	b	42	710,99
	c	42	1482,13

A.3 ENF-GP

Table 12: ENF-GP

Specimen	# Crack	a	GIIc
1	a	36	867,95
	b	32	993,43
	c	32	1099,09
	d	31	1082,53
2	a	32	716,74
	b	40	553,99
	c	29	938,96
	d	42	948,44
	e	31	730,70
3	a	22	557,67
	b	22	340,06
4	a	27	654,10
	b	30	988,80
	c	35	1180,04
	d	36	1436,36
5	a	32	777,78
	b	37	721,55
	c	35	728,09
	d	32	595,78
6	a	37	727,32
	b	37	991,00
	c	37	1589,05
7	a	42	1134,56
	b	42	1330,16
	c	42	1485,66
	d	42	1691,31
	e	42	1641,11

B.1 Matlab code

```
function AreaCalc(data)
clear stop width Area
Area=zeros(11,1);
width = numel(data(1,:));
for m=1:11
clear curve

if 3*m <= width
    length = numel(data(:,3*m));                        %Different lengths
        for i=1:length
              curve(i,[1,2])=data(i,[m*3-1,m*3]);
              if data(i,m*3-1)< 0
                        curve(i,1)=0;                   %Only positive P
              end
              if data(i,3*m)~= 0
                  stop(1,m)=abs(data(i,3*m));           %Get plastic strain
              end
        end
        curve(:,1)=curve(:,1);
        Area(m,1)=trapz(curve(:,2),curve(:,1));         %Get area

    if m > 1
        P(:,m)=curve(:,2)+sum(stop(1,:));               %Move starting point
                                                        with plastic strain

    else
        P(:,m)=curve(:,2);
    end
    D(:,m)=curve(:,1);
else
    P(:,m)=0;
    D(:,m)=0;
end
end

Area
plot(P(:,[1:11]),D(:,[1:11]))
title(inputname(1))
xlabel('Displacement, \Delta [mm]')
ylabel('Load, P [kN]')
```

B.2 Matlab code

```
function ComplianceCalc(data)

clear length loadcurve count x y maxload loadrise top ccurve compliance i
adata
adata(:,:)=abs(data(:,:));
length=numel(data(:,2));
count=1;
maxload=max(adata(:,2));
for i=1:length
    if adata(i,2)>0.1
        loadcurve(count,1)= adata(i,2);
        loadcurve(count,2)= adata(i,4);
        count=count+1;
    end
    if  adata(i,2)== maxload
        loadrise=loadcurve;
    end
end
stop=round(0.7*numel(loadrise(:,1)));
x=loadrise(1:stop,1);
y=loadrise(1:stop,2);
x1=adata(:,4);
y1=adata(:,2);
plot(x1,y1,'b',y,x,'r');
title(inputname(1))
legend('Load curve','Compliance area','Location','SouthEast')
xlabel('Displacement, \Delta [mm]')
ylabel('Load, P [kN]')
ccurve=polyfit(x,y,1);
compliance=ccurve(1,1)
```

C.1 Compliance calibration curves

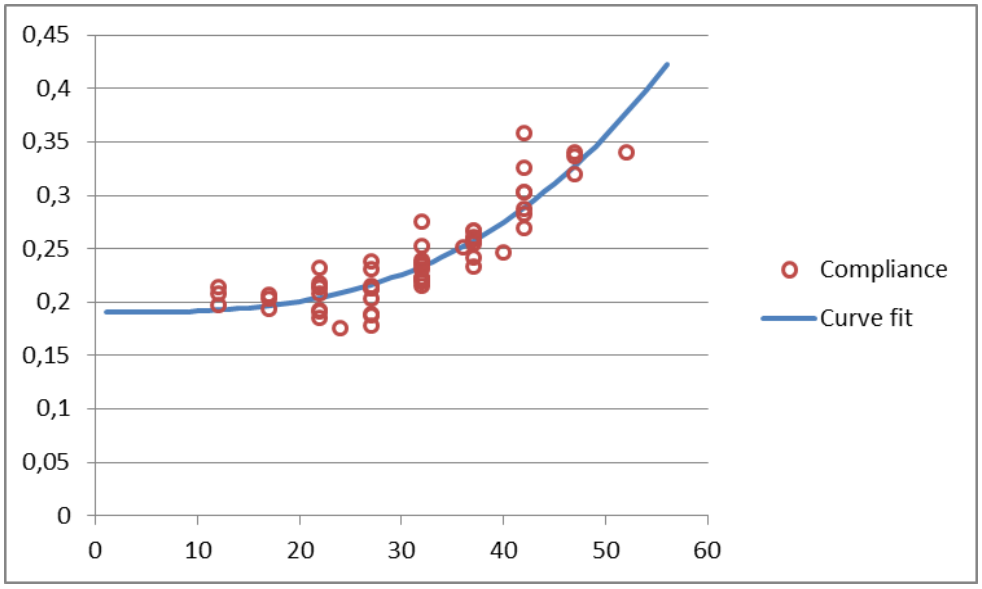

Figure 27: Compliance curve used for calculations ENF-GC

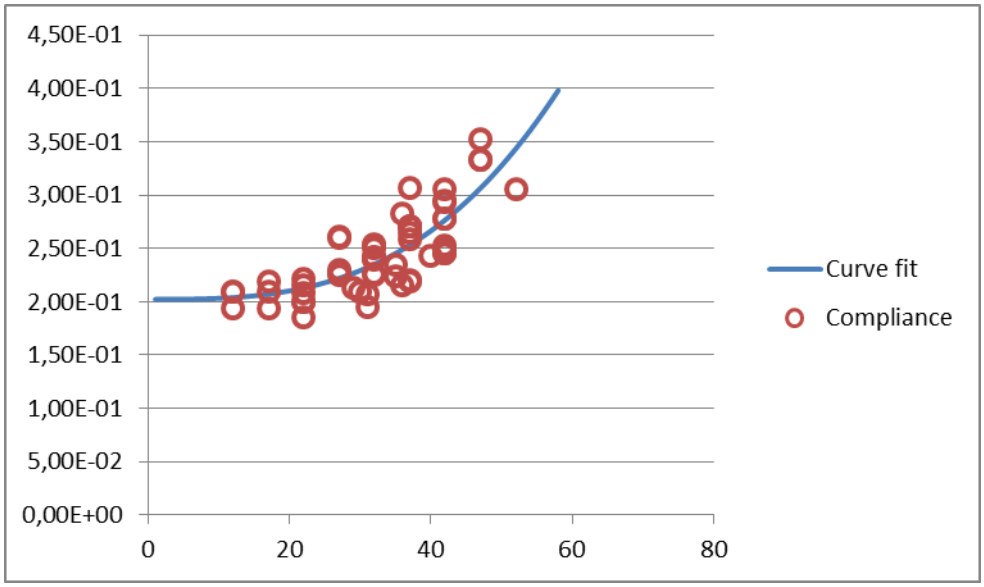

Figure 28: Compliance curve used for calculations ENF-GP

C.2 Compliance calibration comparison

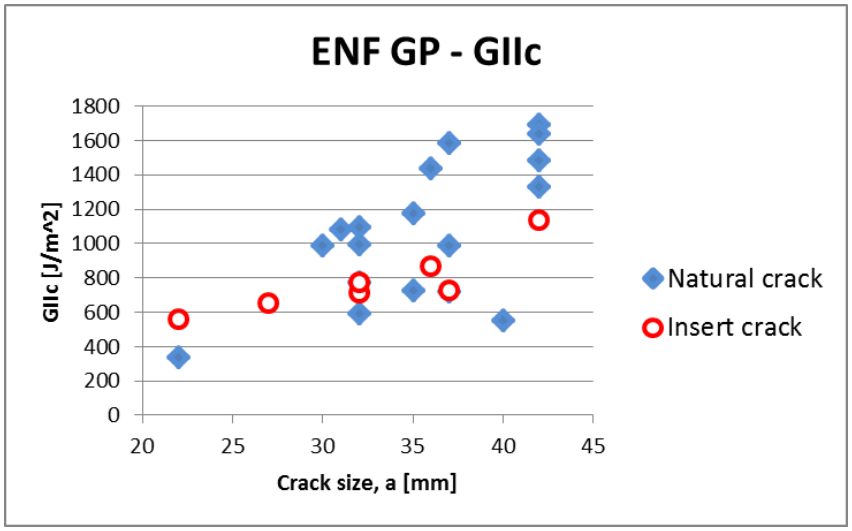

Combined $\mu = 981,\ \sigma = 361$

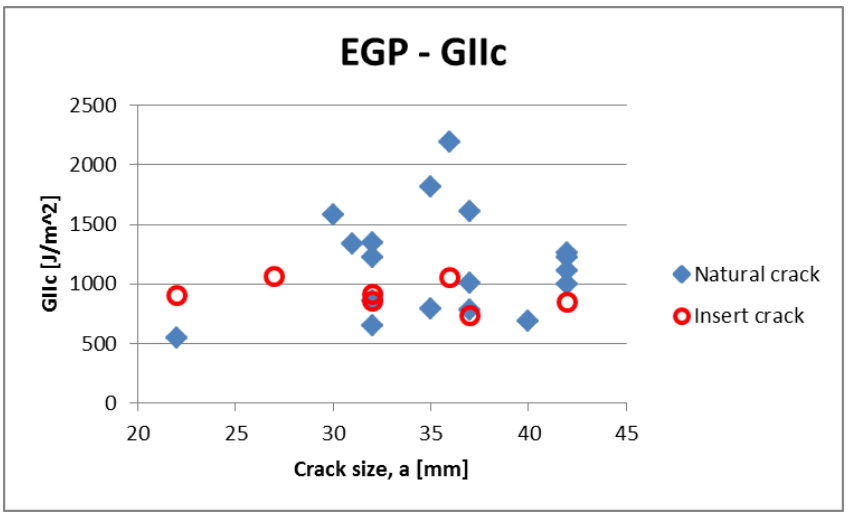

3 point $\mu = 1105,\ \sigma = 373$

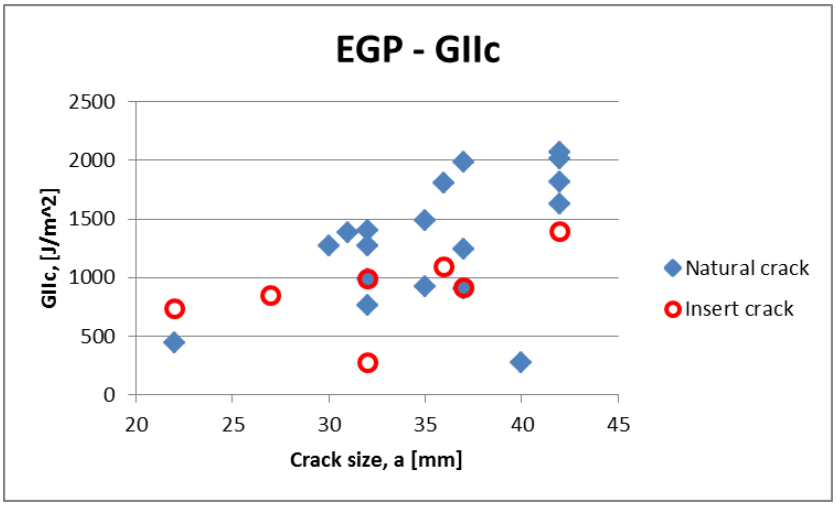

8 point $\mu = 1103,\ \sigma = 572$

Figure 29: Impact of compliance calibration EGP

C.3 Compliance calibration comparison

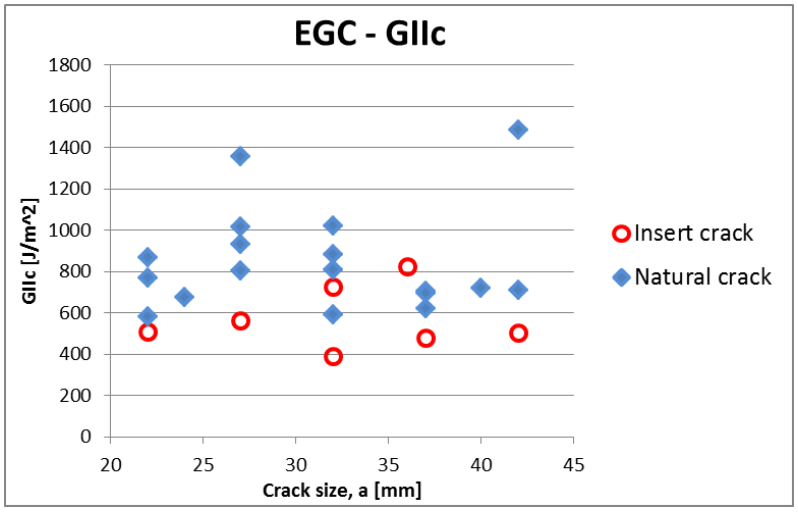

Combined $\mu = 770,\ \sigma = 254$

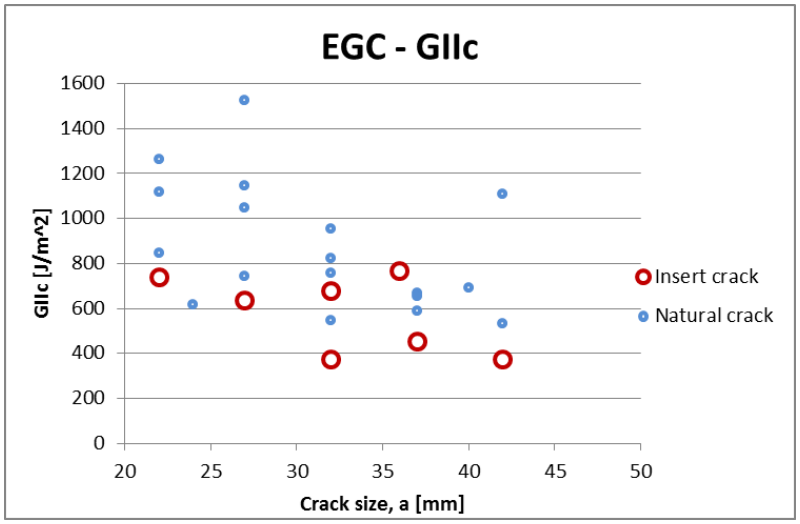

3 point $\mu = 785,\ \sigma = 284$

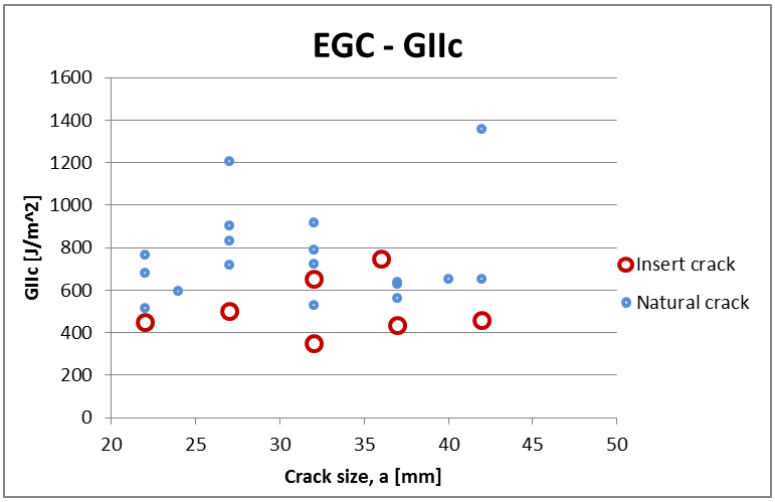

8 point $\mu = 690,\ \sigma = 230$

Figure 30 Impact of compliance calibration EGC

D.1 FEA parameters

Table 13: Parameters for FEA curves

Parameter selection	**Adhesive material**			
	SE84LV		Epikote	
Failure separation	0,1	0,05	0,13	0,1
Penalty stiffness				
Knn	226,00	904,00	315,50	533,20
Ktt	97,60	390,40	56,33	95,20
Ktt	97,60	390,40	56,33	95,20
Interface strength				
Sn	11,30	22,60	20,51	26,66
Stt	4,88	9,76	3,66	4,76
Stt	4,88	9,76	3,66	4,76
Damage evolution, BKK				
Normal mode	0,57	0,57	1,33	1,33
Shear mode	0,24	0,24	0,24	0,24
Shear mode	0,24	0,24	0,24	0,24
Elements				
Carbon Fibre,C3D20R	5	5	5	5
Steel, C3D20R	5	5	5	5
Adhesive, COH3D8	2	2	2	2

Parameters found using energy release rates from testing and equations (5.3) and (5.2)

E.1 Bondline ENF-GC4

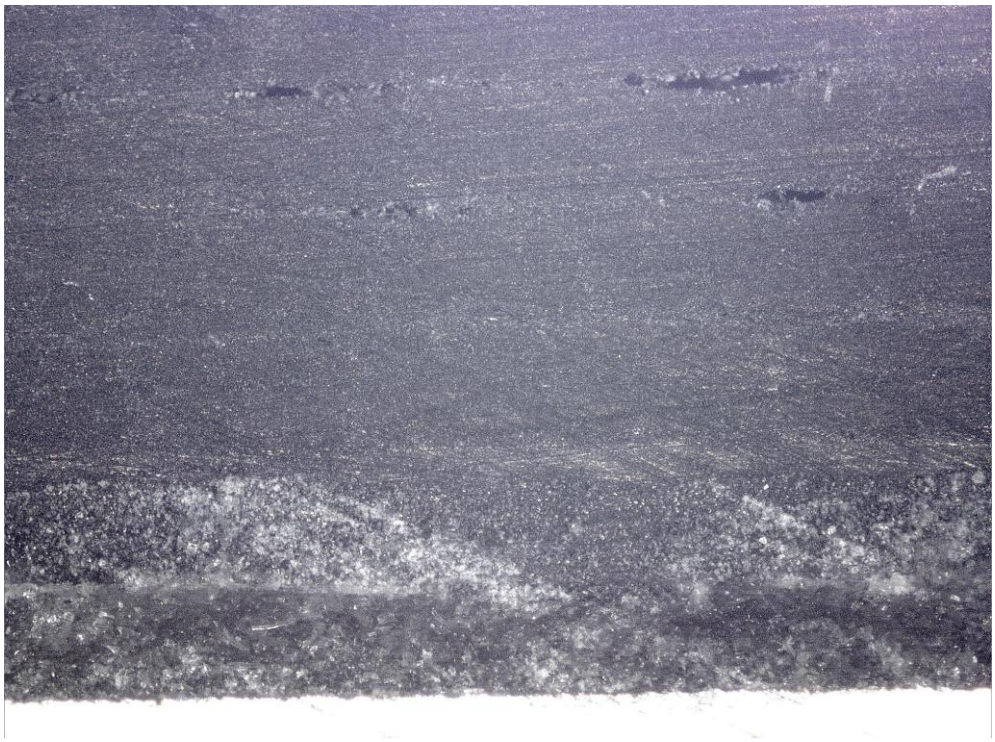

Figure 31: Bondline of ENF-GC4 5x

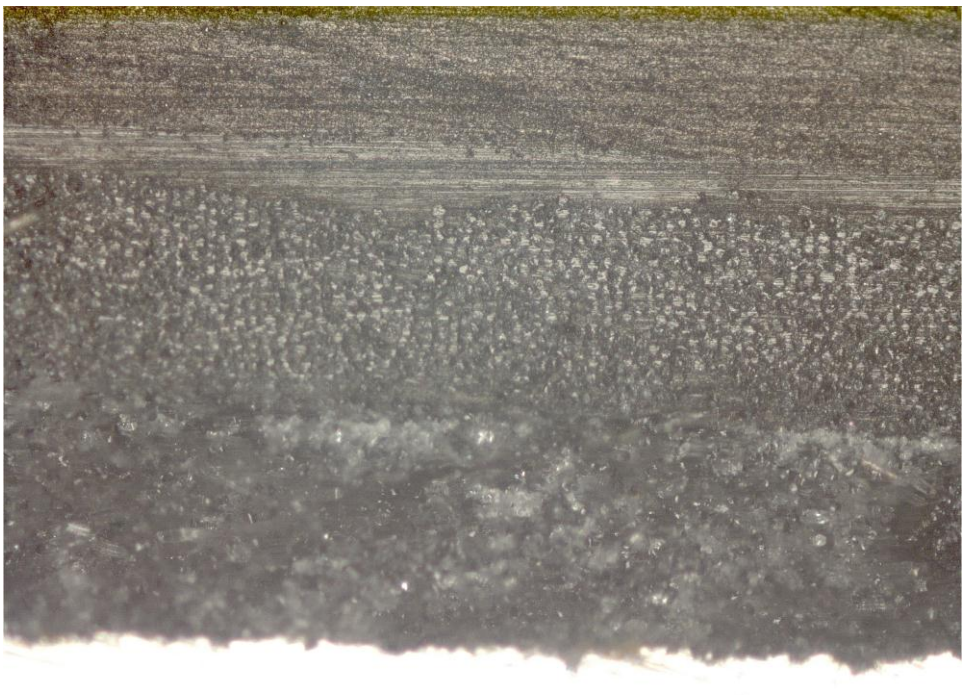

Figure 32 Bondline of ENF-GC4 10x

From the bottom: Steel, glass fiber, carbon fiber. The two layers of the stitched fibers are apparent. No scale is provided.

E.2 Bondline ENF-GP5

Figure 33: Bondline of ENF-GP5 5x

Figure 34: Bondline of ENF-GP5 10x

From the bottom: Steel, glass fiber, carbon fiber. Curvature is evident from the overlapping of weaved glass fibers. No scale was obtained.